Proceedings World Geothermal Congress 2000
Kyushu - Tohoku, Japan, May 28 - June 10, 2000

SEISMIC METHODS FOR OBSERVING GEOTHERMAL FIELD EVOLUTION

J. L. Stevens[1], J. W. Pritchett[1], S. K. Garg[1], K. Ariki[2], S. Nakanishi[3], and S. Yamazawa[4]
[1]Maxwell Technologies, Systems Division, 8888 Balboa Ave., San Diego, CA 92123-1506, USA
[2]Mitsubishi Materials Corporation, 1-297 Kitabukuro-cho, Omiya, Saitama 330-8508, Japan
[3]Electric Power Development Co., Ltd., 6-15-1 Ginza, Tokyo 104-8165, Japan
[4]New Energy and Industrial Technology Development Organization, 3-1-1 Higashi Ikebukuro, Tokyo 170-6028, Japan

Key Words: geothermal, seismic, reservoir modeling

ABSTRACT

Seismic monitoring of a geothermal reservoir is feasible, but it is necessary to design the seismic experiment carefully in order to be able to observe changes in the field. Travel time differences due to changes in the geothermal field with time are estimated to be small – on the order of 10-20 milliseconds. Changes in P velocity and Poisson's ratio over time are large, but occur over small regions of less than a few hundred meters extent leading to the predicted small changes in travel times. Seismic experiments should therefore concentrate on the areas where these differences would be observed. Such changes are likely to be observable in cross-hole surveys, particularly near the regions of injection and the edge of the expanding two-phase zone. The largest effect is due to the presence of steam, which causes a sharp drop in P-velocity, an even sharper drop in Poisson's ratio, strong P-wave attenuation, and seismic reflections from the water/steam boundary. It should, therefore, be possible to map the location and size of the two-phase zone in the producing region of a geothermal reservoir with a well-designed seismic study.

1. INTRODUCTION

This paper is a preliminary assessment of the feasibility of monitoring changes in a geothermal field using seismic methods. To accomplish this, we start with the geothermal model described by Pritchett et al (2000) as a typical model for evolution of a geothermal field, and use theoretical and empirical relations to derive approximate velocity, density, and attenuation models from these calculations. We then calculate the corresponding travel times and amplitudes for seismic waves traveling through these structures, and look at the differences in travel time and attenuation as the geothermal field changes over the 10,000 day period.

Several types of seismic surveys could be used for monitoring a geothermal field, including reflection surveys, refraction surveys, vertical seismic profiling, cross-borehole surveys, or passive seismic surveys using data from local microearthquakes. Each method has advantages and disadvantages with regard to its capability for observing the changes in the field. The observables that can be measured by these surveys are: travel times for P and S waves, and derived quantities such as interval velocity and Poisson's ratio; reflections from parts of the structure with strong velocity contrasts; and attenuation of seismic signals. Attenuation may be measured either as a time domain peak amplitude change, or as changes in spectral shape with attenuation typically being stronger at high frequencies than at low frequencies.

In this feasibility study, we estimate the magnitude of the observables, and the changes in the magnitude of these observables over the life of the geothermal field. From this analysis, an assessment can be made as to which observables are best for identifying changes in the field, which seismic techniques are most effective at measuring them, and whether the changes in the observables will be measurable under realistic conditions found in a typical geothermal field setting.

2. RESERVOIR VELOCITY ESTIMATE

The geothermal reservoir simulation yields temperature, gas and water content over a three-dimensional grid for a 10,000-day interval, with intermediate calculations done at intervals of 0, 1000, 2000, and 5000 days. Time zero corresponds to the state of the field in its "natural state" prior to start of production or injection. The quantities included in the original model that are relevant to the seismic calculation are temperature, porosity, water saturation, steam saturation, rock density, and temperature dependent water and steam velocity and density.

The velocity model is derived in the following way: first, we use parameters for rock velocity and density that are consistent with our experience in geothermal fields; second, we use empirical relations to derive related quantities; and third, we use Biot theory to calculate the mixed phase (rock/water/steam) velocity. We start with the observation that velocity usually increases with depth, and use a dry rock grain velocity that increases from 4000 m/sec at the surface to 6000 m/sec at the 3 km depth of the bottom of the grid. These numbers are typical of a geothermal field, and our calculations showed that although the observables (travel time and attenuation) are sensitive to these values, the changes in the observables are not sensitive to assumptions about the rock velocities.

The rock density ρ_r is estimated from the velocities V_r using Gardner's relation (Gardner et al., 1974; Sheriff and Geldart, 1983) $\rho_r=310\ V_r^{1/4}$ kg/m^3. This leads to densities in the model ranging from 2465 kg/m^3 to 2728 kg/m^3. A constant density of 2500 kg/m^3 was assumed in the original model. The grain bulk modulus is calculated using the approximation $K_r=0.9\rho_r V_r^2$, Porous rock is more compliant and therefore has a lower velocity than the rock grains themselves. Based on typical values of rock moduli from geothermal fields, we set the bulk modulus of porous rock $K_p=K_r/4$, and set the shear modulus of the porous rock $\mu=K_r/6$. Velocity also decreases with increasing temperature. Based on data for dry sandstone in Gregory (1977), we model the temperature effect by reducing the elastic moduli by 7% per 100°C, which corresponds to a velocity decrease of about 3% per 100°C.

Biot theory (Gregory, 1977; Garg and Nayfeh, 1986) is used to calculate the velocities of the liquid/solid/gas mixture. To a very good approximation, if the gas (steam) content is nonzero, then the rock/fluid mixture bulk modulus K_m is equal to K_p. If the steam content is zero, then the following relation holds (K_f is the fluid bulk modulus):

$$K_m = K_p + (1 - K_p/K_r)^2 \{\varphi/K_f + (1-\varphi)/K_r - K_p/K_r^2\}^{-1}$$

where φ is the porosity. The density ρ_m of the water/gas filled rock is given by:

$$\rho_m = (1-\varphi)\rho_r + \varphi(1-S)\rho_f + \varphi S\rho_g$$

where ρ_f is the fluid density, ρ_g is the gas density, and S is the steam saturation. The porous velocity V_p is then given by

$$V_p = [(K_m + 4/3\ \mu)/\rho_m]^{1/2}$$

For the geothermal calculation, this leads to velocities that range from 2785 m/sec to 4340 m/sec. The range of the velocities changes very little over the 10,000 day time period of the calculation, however the distribution of the velocities throughout the structure varies substantially. In particular, regions where steam develops have significantly lower velocities than regions containing no steam, and the region containing steam expands substantially as the reservoir is exploited.

2. SEISMIC TRAVEL TIMES

The observed seismic travel times depend on how the travel times are measured, and in particular on the ray paths between the source and receiver. Since low velocity regions are concentrated in relatively narrow depth range, for example, travel times through this region are minimized for vertically incident rays as would occur in a passive seismic experiment, and the effect will be larger for horizontal waves as could occur with a crosshole or VSP experiment. Our main interest here is to get an estimate of the magnitude of the effect, so we have modeled the simple case of vertically incident waves coming up through the bottom of the grid similar to a passive seismic experiment. Figure 1 shows the calculated travel times for these rays in the initial equilibrium state, and after 10,000 days of production.

Although the differences in the total travel time through the initial and final model are small, there are significant differences in the way the travel times are distributed. In particular the region containing steam has expanded and changed in shape, differing from the initial cylindrical symmetry, the injection region is clearly visible as a region of shorter travel times, and there has been an overall cooling and corresponding reduction of travel times over the lifetime of the field. This is illustrated in Figure 2, which shows the magnitude of the travel time differences between the initial and final model. The travel time differences range from a decrease of about 15 milliseconds to an increase of about 3 milliseconds. These differences are small, but could be observed in a carefully planned experiment.

The discussion above concerned the evolution of the field from the initial state to the final state. We now look at the state of the field at intermediate times to see if these changes are observable. Figure 3 through Figure 6 show the travel time differences between each of the time steps in the calculation. Several significant features of field evolution can be seen in these figures. The first 1000 days of production are characterized by a pronounced heating of the production region and cooling of the injection region with travel times increased and decreased, respectively. From 1000 to 2000 days, the production and injection regions both cool, and the steam bubble expands. These effects continue from 2000 to 5000 days. From 5000 to 10000 days there is an overall cooling and corresponding travel time reduction throughout the field except near the southwest edge of the reservoir where some increased travel times due to the expanding steam bubble can be observed.

3. CHANGES IN VELOCITY AND POISSON'S RATIO

The travel time changes discussed in the last section are caused by changes in seismic velocities in localized areas due to heating, cooling, and the presence or absence of steam. The same factors cause changes in shear velocity, except that shear velocity is much less sensitive to the presence of steam. Poisson's ratio ν, which is derived from the P and S velocities V_p and V_s through the relation $\nu = (V_p^2-2V_s^2)/(V_p^2-V_s^2)/2$ is therefore also sensitive to these factors and will decrease significantly if steam is present. In the example studied here, the P velocities range from 2785 m/s to 4340 m/s, the shear velocities range from 1655 m/s to 2229 m/s and Poisson's ratio ranges from 0.227 to 0.336.

The following figures show the changes in P velocity and Poisson's ratio over the lifetime of the field and depths between 375 and 750 meters in the structure. Figures 7 and 8 show the changes between 625 and 750 meters depth; Figures 9 and 10 between 500 and 625 meters, and figures 11 and 12 between 375 and 500 meters. Some of the changes are quite dramatic. Near the point of injection, P velocity increases by as much as 10% and Poisson's ratio increases by almost 20%. At the edge of the steam bubble, the P-velocity decreases by about 5% and Poisson's ratio decreases by about 15%. These numbers show that velocity changes and particularly Poisson's ratio changes are large enough to be easily observable in an experiment designed to detect them. Because these changes occur over a small volume it is necessary to perform controlled experiments with good time resolution. Cross-hole surveys, for example, would be an ideal way to observe these changes.

4. ATTENUATION

Regions containing a mixture of steam and water are also characterized by high P-wave attenuation. . Romero et al. (1997) studied the variability in attenuation in the region around the Geysers geothermal field in California, and report that in a steam-bearing region the P-wave attenuation Q_p^{-1} is increased much more than the S-wave attenuation Q_s^{-1} compared to surrounding areas. Ito et al. (1979) using data on Massilon sandstone from Winkler and Nur (1979) show that the P-wave attenuation Q_p^{-1} is as high at 0.04 for partially saturated rock at pressures typical of geothermal fields. However Q_p^{-1} drops to less that 0.01 for fully saturated rock and as low as 0.002 for dry rock. The S-wave attenuation Q_s^{-1} is as high as 0.02 for both fully saturated and partially saturated rock, but drops to about 0.005 for dry rock. The high P-wave attenuation provides another way of observing regions of steam in a geothermal field. Romero et al. (1997) report Q_p^{-1} measurements as high as 0.1 above a background Q level in the Geysers geothermal reservoir. Q_p^{-1} values can be inferred from spectral ratios using both spectral shape and amplitude. For example, spectral ratios of P-waves observed from local earthquakes propagating through the geothermal field can be used to estimate the attenuation of the signals which can then be used to identify areas containing steam.

To estimate the magnitude of this effect, we calculated the attenuation of signals traveling through the geothermal example field discussed in the previous sections. The amplitude of signals traveling through the structure is given by

$$A = A_o \exp\left[-\int \frac{\pi f}{Q_p V_p} dx\right]$$

where A_0 is the amplitude at the bottom of the structure and the integral is over the path through the structure, and f is the frequency. For purposes of this example, we calculate the ratio of the amplitude at the top of the structure relative to the amplitude at the bottom for a frequency of 1 Hz using Q_p^{-1} =0.04 for regions containing steam, and 0.01 for fully saturated regions with no steam. The following figures show the quantity

$$\log_{10}\left(\frac{A_o}{A}\right) = \pi f \left(\log_{10} e\right) \int \left(Q_p V_p\right)^{-1} dx$$

integrated from the bottom to the top of the structure for f=1. Since the ratio is proportional to frequency all of the numbers scale with frequency, so for example the maximum attenuation of 0.03 (7% reduction in amplitude) at one Hz corresponds to an attenuation of 3 (reduction in amplitude by a factor of 1000) at 100 Hz. Figure 13 shows the attenuation of the geothermal field in its natural state and Figure 14 shows the attenuation after 10,000 days of field operation. Figure 15 shows the change in attenuation over the 10,000 day lifetime of the field. Similar to the previous results with velocity and travel time, the prominent features are increased attenuation in the region of the expanding steam bubble, and decreased attenuation near the region of injection. The maximum change in attenuation is about 15% of the maximum attenuation, which should be large enough to be measurable in a carefully planned experiment.

5. MEASUREMENT OF SEISMIC OBSERVABLES

Based on this analysis, we can draw the following conclusions regarding the magnitude of the seismic observables.

Changes in velocity and Poisson's ratio with time – local velocity changes can be as large as 10% and Poisson's ratio as large as 20% over the lifetime of the field. These changes are large enough to be easily observable with the right kind of experiment, however because these large changes in velocity occur over small regions of a few hundred meters or less, the experiments must be chosen to have good time resolution and relatively short paths. Cross-hole surveys would probably be the ideal type of measurement for observing these changes.

Travel times - The maximum travel time differences expected over the life of the field are about 20 milliseconds. In order to have adequate resolution to see details of the field changes, travel time accuracy of about 1 millisecond is required. While this is a strong constraint, it should be achievable with a well thought out seismic experiment. For example, since the most easily observable and potentially most interesting effect is the size and location of the steam bubble, an experiment could be designed to focus on the region near the edge of the steam bubble and to monitor it as a function of time. This change might be observed by examining the location of a basement reflector beneath the field, which would appear to move up and down as the velocity field above it increased or decreased.

Spatial changes in velocity - The velocity change due to the presence or absence of steam is a strong effect. A typical velocity change would be a drop from about 2950 m/sec to 2800 m/sec for a region changing from no steam to some steam. This change is about 5%, which represents a fairly strong contrast. For a region with a thickness of 500 meters, this change corresponds to a travel time difference of about 9 milliseconds.

Reflections – A velocity change of a few percent, as occurs at a steam/no steam boundary, is large enough to cause a significant reflection. The amplitude of the reflected ray at a 5% velocity change is approximately 2.5% of the incident amplitude. Monitoring a geothermal field with a reflection survey or other experiment that looked for reflections could monitor the boundary of the steam bubble over time.

Attenuation - P-wave attenuation is strongly affected by gas and water content, with particularly strong attenuation when gas is present. Strong attenuation and the difference between P and S attenuation can therefore be used to map steam bearing regions. For the example studied in this report, we estimate a change in attenuation over the lifetime of the field of about 15% of the maximum attenuation. This number should be regarded as approximate because the attenuation rate can vary substantially depending on the type of material and other conditions of the geothermal field. Observation studies of the Geysers geothermal field show attenuation stronger than this estimate. All studies indicate that P-wave attenuation is a strong effect that can be used to monitor changes in a geothermal field.

6. SUMMARY

Seismic monitoring of a geothermal reservoir is feasible, but it is necessary to design the seismic experiment carefully in order to be able to observe changes in the field. Travel time differences due to the presence of a geothermal reservoir are predicted to be on the order of tenths of seconds, and therefore easily observable. Changes in the geothermal field with time are estimated to be much smaller – on the order of 10-20 milliseconds. Changes in P velocity and Poisson's ratio over time are large, but occur over small regions of less than a few hundred meters extent leading to the predicted small changes in travel times. Seismic experiments should therefore concentrate on the areas where these differences would be observed. Cross-hole surveys, particularly near the regions of injection and the edge of the expanding steam bubble are likely to produce data with the necessary resolution. The largest effect is due to the presence of steam, which causes a sharp drop in P-velocity, an even sharper drop in Poisson's ratio, strong P-wave attenuation, and seismic reflections from the water/steam boundary. It should, therefore, be possible to map the location and size of the steam bubble in the producing region of a geothermal reservoir with a well-designed seismic study.

ACKNOWLEDGEMENT

NEDO supported this work as part of the "New Sunshine Project" sponsored by the Agency of Industrial Science and Technology (AIST) of the Japanese Ministry of International Trade and Industry (MITI).

REFERENCES

Gardner, G. H. F., Gardner, L. W., and Gregory, A. R. (1974), "Formation velocity and density – the diagnostic basics for stratigraphic traps," *Geophysics*, **16**, pp. 673-685.

Garg, S. K. and A. H. Nayfeh (1986), "Compressional wave propagation in liquid and/or gas saturated elastic porous media," *J. Appl. Phys*., **60**, pp. 3045-3055.

Gregory, A. R. (1977), "Aspects of rock physics from laboratory and log data that are important to seismic interpretation," in *Seismic Stratigraphy – Applications to Hydrocarbon Exploration*, pp. 15-46 (ed. C. E. Peyton), Tulsa, AAPG Memoir 26.

Ito, H., J. DeVilbiss, and A. Nur (1979), "Compressional and shear waves in saturated rock during water-steam transition," *J. Geophys. Res*., **84**, pp. 4371-4735.

Pritchett, J., J. L. Stevens, P. Wannamaker, S. Nakanishi, and S. Yamazawa (2000), "Theoretical Feasibility Studies of Reservoir Monitoring Using Geophysical Survey Techniques," *Proc. World Geothermal Congress 2000*, Japan (in press).

Romero, A. E., T. V. McEvilly, and E. L. Majer (1997), "3-D microearthquake attenuation tomography at the Northwest Geysers geothermal region, California," *Geophysics*, **62**, pp. 149-167.

Sheriff, R. E. and L. P. Geldart (1983), *Exploration Seismology, Volume 2: Data Processing and Interpretation*, Cambridge University Press, New York.

Winkler, K. and A. Nur (1979), "Pore fluids and seismic attenuation in rocks," *Geophys. Res. Lett*., **6**, pp. 1-4.

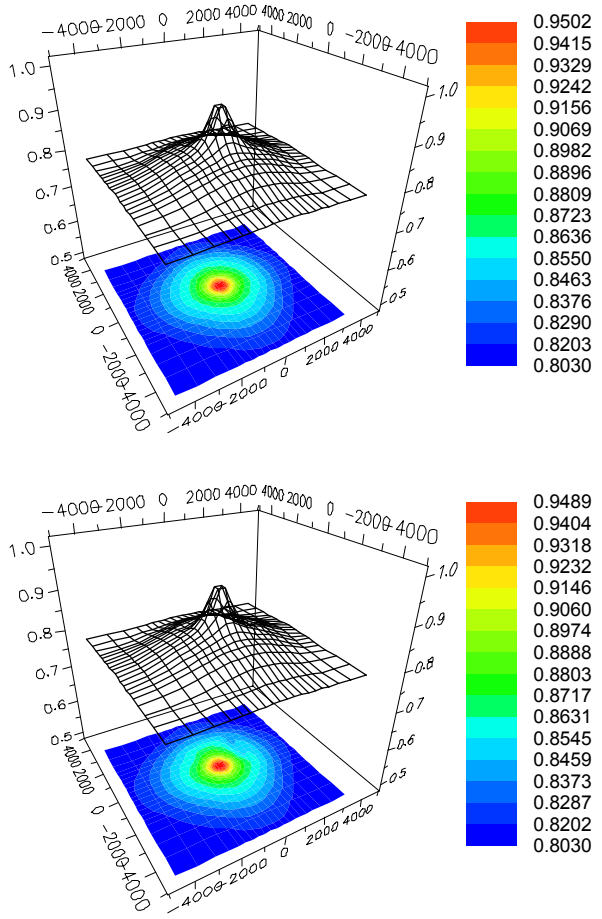

Figure 1. Vertical travel times through the 3000 meter thick geothermal grid in its initial equilibrium state (Top) and final state after 10,000 days (Bottom). In all figures, travel time is for the P wave in seconds, and distance is in meters.

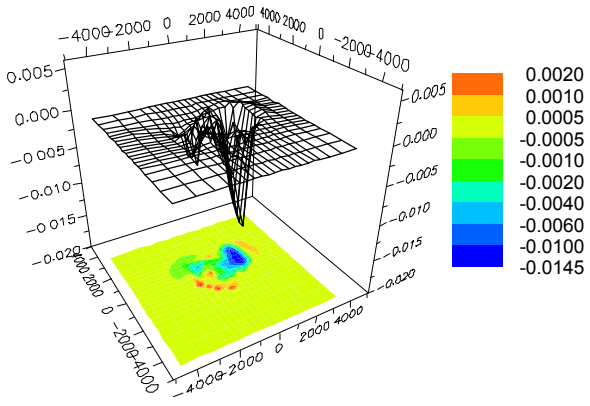

Figure 2. Travel time differences between zero and 10,000 days. The deep negative region corresponds to injection, and the high amplitude region corresponds to the edge of the steam bubble which has expanded over this time period.

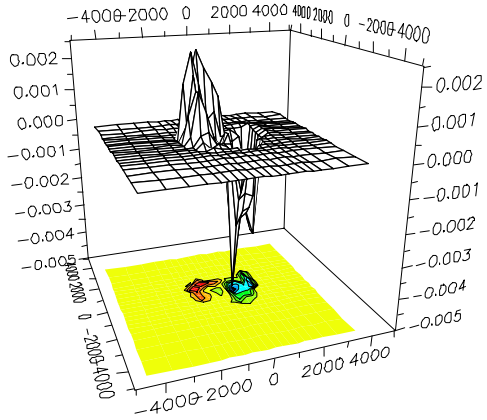

Figure 3. Travel time differences between zero and 1000 days.

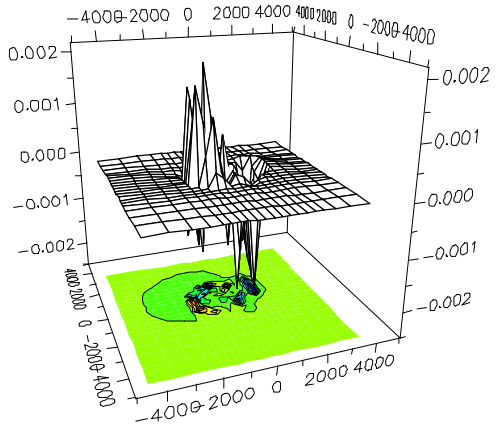

Figure 4. Travel time differences between 1000 and 2000 days.

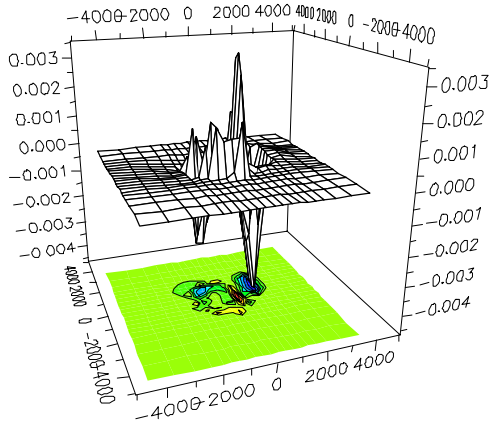

Figure 5. Travel time differences between 2000 and 5000 days.

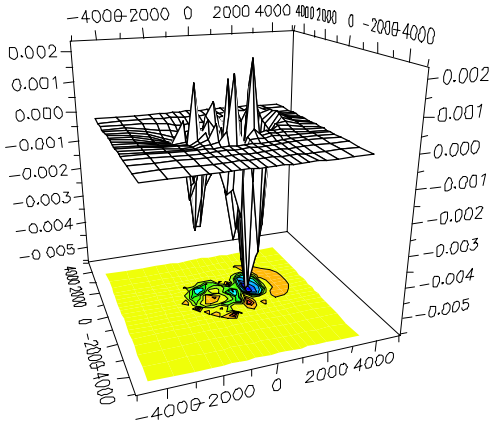

Figure 6. Travel time differences between 5000 and 10,000 days.

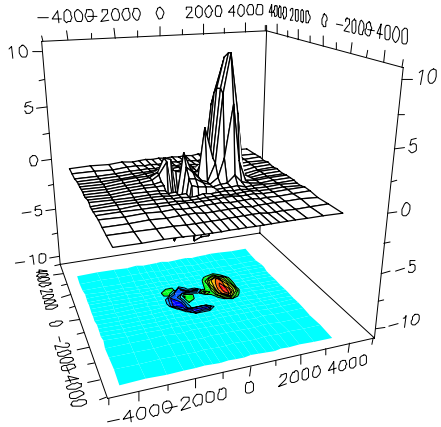

Figure 7. Depth 625-750 meters, Velocity change after 10,000 days (%).

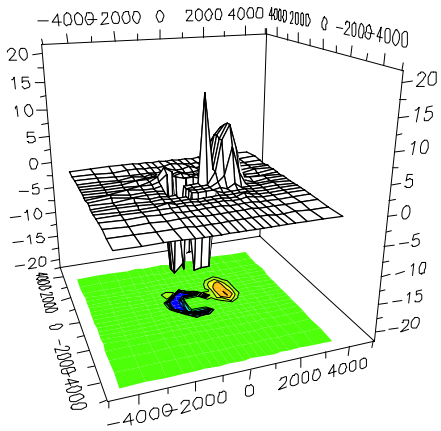

Figure 8. Depth 625-750 meters, Poisson's ratio change after 10,000 days (%).

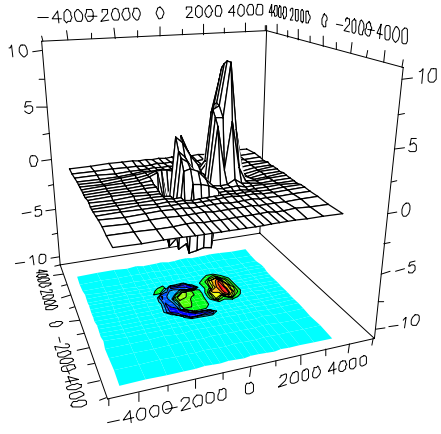

Figure 9. Depth 500-625 meters. Velocity change after 10,000 days (%).

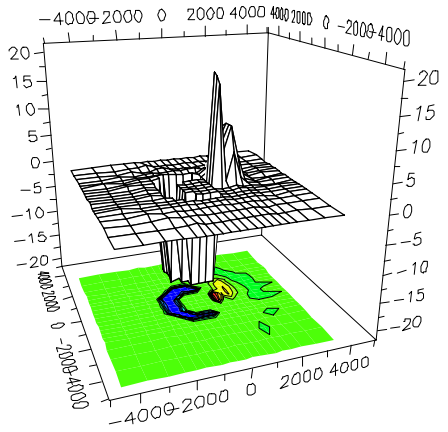

Figure 10. Depth 500-625 meters Poisson's ratio change after 10,000 days (%).

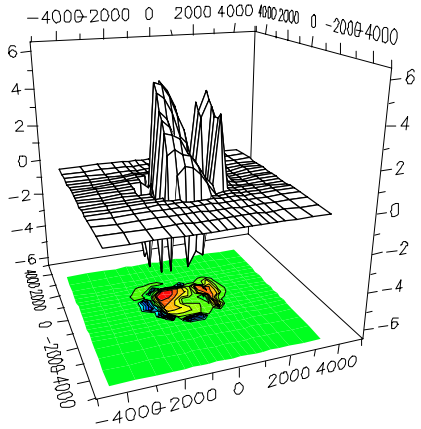

Figure 11. Depth 375-500 meters. Velocity change after 10,000 days (%).

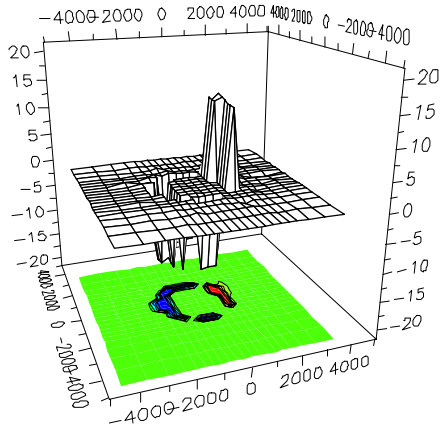

Figure 12. Depth 375-500 meters. Poisson's ratio change after 10,000 days (%).

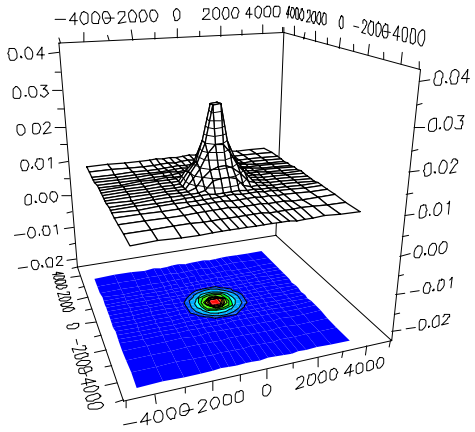

Figure 13. Log attenuation of 1 Hz rays traveling vertically through the geothermal field in its natural state. Log attenuation is defined as the logarithm of the amplitude ratio between the bottom and the top of the structure. Log attenuation scales linearly with frequency, so the numbers are multiplied by a factor of 100 at 100 Hz.

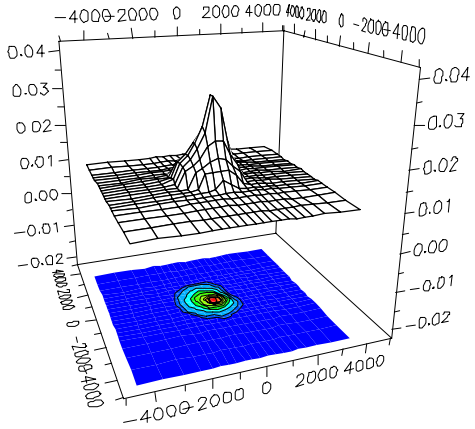

Figure 14. Log attenuation of rays traveling vertically through the geothermal field after 10,000 days of operation.

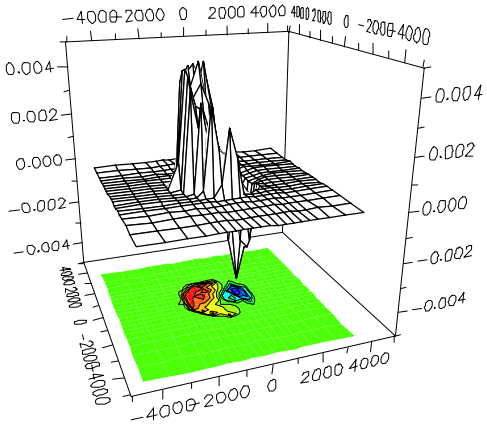

Figure 15. Change in log attenuation through the geothermal field after 10,000 days of operation.